Title

Single Tryptophan and Tyrosine Comparisons in the N-Terminal and C-Terminal Interface Regions of Transmembrane GWALP Peptides

Journal

The Journal of Physical Chemistry B, 117(44)

ISSN

1520-6106

Authors

Gleason, Nicholas J
Greathouse, Denise V
Grant, Christopher V
et al.

Publication Date

2013-11-07

DOI

10.1021/jp407542e

Peer reviewed

Published in final edited form as:
J Phys Chem B. 2013 November 7; 117(44): 13786–13794. doi:10.1021/jp407542e.

Single Tryptophan and Tyrosine Comparisons in the N-terminal and C-terminal Interface Regions of Transmembrane GWALP Peptides†

Nicholas J. Gleason[1], **Denise V. Greathouse**[1], **Christopher V. Grant**[2], **Stanley J. Opella**[2], and **Roger E. Koeppe II**[1,*]

[1]Department of Chemistry and Biochemistry, University of Arkansas, Fayetteville, AR 72701

[2]Department of Chemistry and Biochemistry, University of California, San Diego; La Jolla, CA 92093

Abstract

Hydrophobic membrane-spanning helices often are flanked by interfacial aromatic or charged residues. In this paper we compare the consequences of single Trp → Tyr substitutions at each interface for the properties of a defined transmembrane helix, in the absence of charged residues. The choice of molecular framework is critical for these single-residue experiments, because the presence of "too many" aromatic residues (more than one at either membrane-water interface) introduces excess dynamic averaging of solid-state NMR observables. To this end, we compare the outcomes when changing W^5 or W^{19}, or both of them, to tyrosine in the well characterized transmembrane peptide acetyl-GGALW^5(LA)$_6$LW^{19}LAGA-amide ("GWALP23"). By means of solid-state ^{2}H and ^{15}N NMR experiments, we find that $Y^{19}GW^5$ALP23 displays similar magnitudes of peptide helix tilt as Y^5GW^{19}ALP23 and responds similarly to changes in bilayer thickness, from DLPC to DMPC to DOPC. The presence of Y^{19} changes the azimuthal rotation angle ρ (about the helix axis) to a similar extent as Y^5, but in the opposite direction. When tyrosines are substituted for both tryptophans to yield GY^{5,19}ALP23, the helix tilt angle is again of comparable magnitude, and furthermore the preferred azimuthal rotation angle ρ is relatively unchanged from that of GW^{5,19}ALP23. The extent of dynamic averaging increases marginally when Tyr replaces Trp. Yet, importantly, all members of the peptide family having single Tyr or Trp residues near each interface exhibit only moderate and not highly extensive dynamic averaging. The results provide important benchmarks for evaluating conformational and dynamic control of membrane protein function.

Keywords

deuterium and ^{15}N solid-state NMR; lipid bilayer; GALA analysis; aromatic residues at the membrane interface

†This work was supported in part by NSF MCB grants 0841227 and 1327611, and by the Arkansas Biosciences Institute. The peptide facility is supported by NIH grants GM103429 and GM103450. The ^{2}H NMR facility in Fayetteville AR was supported by NIH grant GM103450. The ^{15}N NMR facility in La Jolla CA was supported by the Biotechnology Research Center for NMR Molecular Imaging of Proteins at the University of California, San Diego, which is supported by NIH grant P41EB002031.

Address correspondence to: Roger E. Koeppe II, Tel. (479) 575-4976; Fax. (479) 575-4049; rk2@uark.edu.

SUPPORTING INFORMATION AVAILABLE. Additional NMR spectra, mass spectra, CD spectra, fluorescence spectra, chromatograms, and helix azimuthal rotation plots. This material is available free of charge via the Internet at http://pubs.acs.org.

1. INTRODUCTION

The heterogeneous lipid bilayer environment presents challenges for characterizing the properties of membrane proteins. The bilayer membrane can alter protein dynamics, regulate enzyme and transport activity, and influence other protein functions [1–5]. Concurrently, membrane proteins can have noticeable effects on the bilayer itself, at times altering bilayer thickness, fluidity, curvature and even the lipid phase [6–9]. With many variables acting simultaneously, it becomes important to understand how individual features contribute to the collective system. For better understanding of the orientations and dynamic interactions between transmembrane helix segments and the lipid bilayer, model peptide sequences such as WALP-family peptides [9,10] and more recently GWALP23 (acetyl-GGALW^{5}(LA)$_{6}$LW^{19}AGA-amide) [11,12] have been used to establish common rules and allow systematic approaches to properties such as hydrophobic matching and the importance of "anchoring" residues [13–15]. Nevertheless, a number of contributing factors may govern the properties of even "simple" model peptides within the bilayer. For example, the peptide acetyl-G**R**ALW^{5}(LA)$_{6}$LW^{19}A**R**A-amide can be seen to increase systematically its tilt as the bilayer thins, to compensate for hydrophobic mismatch when the peptide contains a single Trp residue and a second charged residue within each membrane interface, flanking the core hydrophobic helix [12,16]. But upon addition of a second Trp near each terminal (replacing the **R** residues, above), the peptide dynamics increase dramatically [16], suggesting complex interfacial interactions for the aromatic residues. Also the apparent loss of response to bilayer thickness suggests that hydrophobic "mismatch" may play a secondary role to dynamic considerations and Trp-interface interactions, as has been additionally observed in other model systems [17]. Indeed, in the context of physiologically important transmembrane proteins, it has been confirmed through sequence surveys and statistical analysis that aromatic residues are preferentially found at the water-lipid interface regions [18–20].

It is important to make direct comparisons between interfacial Trp and Tyr substitutions in membrane proteins because both of these aromatic residues are amphipathic and able to form hydrogen bonds; yet their sizes differ, and their detailed lipid interactions could be different. Indeed, the single-channel conductances and especially the open-state lifetimes of gramicidin channels differ substantially when tyrosines are substituted for tryptophans,[21] indicating different functional interactions of Tyr and Trp at a membrane/water interface. In this context, the detailed effects of single substitutions on biophysical properties need to be determined. An added reason for such a study of detailed effects is the increasing use of molecular dynamics simulations to study peptides in membranes. Indeed, detailed experimental data are needed to test the force fields that are developed and used for simulations. Previously, we characterized the impact of changing the N-terminal W^{5} anchor in GWALP23 to Y^{5}, and of introducing a second tyrosine to give the double-Tyr mutant Y^{4,5}GWALP23 [22]. While the single Y^{5} substitution yielded nearly identical peptide behavior (only a rotation of ~10° about the helix axis), the Y^{4,5} peptide experienced markedly increased dynamic averaging of NMR observables, behavior that was reminiscent of previous WALP sequences that incorporated multiple aromatic (Trp) anchors on both ends of the peptide. To further assess the similarities and differences between Trp and Tyr as interfacial aromatic anchoring residues, we have substituted the W^{19} with Y^{19} in GWALP23, to obtain Y^{19}GW^{5}ALP23. Within this context, one notes that the side-chain torsion angles that promote interfacial hydrogen bonding will be different at the N- and C-termini [15,23]. Tyrosine placement furthermore has been observed to be more common at the C-terminus than at the N-terminus of single-span helical segments of transmembrane proteins [18]. In addition to comparing the N- and C-terminal tyrosine placements, we examine the properties of GY^{5,19}ALP23, in which both tryptophans of GWALP23 are replaced with tyrosine.

2. MATERIALS AND METHODS

Commercial L-alanine-d_4 from Cambridge Isotope Laboratories (Andover, MA) was modified with an Fmoc group, as described previously [24], and was recrystallized from ethyl acetate:hexane, 80:20. NMR spectra (^{1}H) were used to confirm successful Fmoc-Ala-d_4 synthesis. Fmoc-L-Ala-^{15}N and Fmoc-L-Leu-^{15}N were purchased from Cambridge. Other protected amino acids and acid-labile "Rink" amide resin were purchased from NovaBiochem (San Diego, CA). All peptides were synthesized on 0.1 mmol scale as described previously [22]. Typically, two deuterated alanines of differing isotope abundances were incorporated into each synthesized peptide. A total of six deuterated alanines, two each in three separately synthesized samples of each peptide, were used for the ^{2}H NMR analysis. Some peptides were synthesized without deuterium, but with 100% abundance of ^{15}N in selected residues. The final residue on each peptide was acetyl-Gly to yield a blocked, neutral N-terminal. Peptides were purified as described [25,26], using an octyl silica column (Zorbax Rx-C8, 9.4 × 250 mm, 5 μm particle size; Agilent Technologies, Santa Clara, CA) and a gradient of 96–100% methanol (with 0.1% trifluoroacetic acid) over 28 min. Peptide identity and purity were confirmed by mass spectrometry and reversed-phase HPLC analysis (Figures S1–S2 of the Supporting Information).

Mechanically aligned samples for solid-state NMR spectroscopy (1/60, peptide/lipid, mol/mol) were prepared using DOPC, DMPC or DLPC lipids from Avanti Polar Lipids (Alabaster, AL), and deuterium-depleted water (Cambridge; 45% w/w hydration), as described previously [22,27]. Bilayer alignment within each sample was confirmed using ^{31}P NMR at 50 °C on a Bruker Avance 300 spectrometer (Billerica, MA) at both $\beta = 0°$ (bilayer normal parallel to magnetic field) and $\beta = 90°$ macroscopic sample orientations (Figure S3 of the Supporting Information). Deuterium NMR spectra were recorded at 50 °C using both sample orientations on a Bruker Avance 300 spectrometer, utilizing a quadrupolar echo pulse sequence [28] with 90 ms recycle delay, 3.2 μs pulse length and 115 μs echo delay. Between 0.6 and 1.5 million scans were accumulated during each ^{2}H NMR experiment. An exponential weighting function with 100 Hz line broadening was applied prior to Fourier transformation.

Magnetically oriented bicelles for solid-state ^{15}N NMR spectroscopy (1/80, peptide/total lipid) were prepared using DMPC-ether and DHPC-ether lipids (3.2/1.0, mol/mol; "q" value) from Avanti Polar Lipids (Alabaster, AL), in a total volume of 175 μL deuterium-depleted water (Cambridge). (The ether lipids, particularly the short-chain DHPC-ether, offer the significant advantage of added chemical stablility over the corresponding ester lipids in bicelle samples [29].) Furthermore, we have observed that the peptide tilt and NMR observables are not appreciably influenced by the choice of ether or ester linkage [16,23].) Peptide and DHPC-ether were mixed and then dried under nitrogen flow and vacuum to remove organic solvent. Separate samples of the DMPC-ether lipid also were prepared in aliquots and dried. Peptide/DHPC-ether films were hydrated using 100 μL water, and DMPC-ether with 75 μL water. After the contents of two separate vials were dissolved, the peptide/DHPC-ether solution was transferred to the DMPC-ether solution. Contents were cycled between 0 °C and 45 °C several times, with intermittent vortexing, until the solution remained clear when cold. While still cold, the bicelle sample solution was transferred to a 5 mm NMR tube and sealed.

For ^{15}N-based SAMPI4 experiments (in the same family of pulse sequences as PISEMA), Y^{19}GWALP23 and Y^{5}GWALP23 enriched in ^{15}N leucine and alanine were synthesized (five labels, residues 13–17). ^{15}N chemical shifts and ^{15}N-^{1}H dipolar coupling values were recorded using a 500 MHz Bruker Avance spectrometer and established pulse sequences [30–33], as described previously [22]. The bicelle sample temperature was maintained at 42 °C, just below a critical temperature for structural transformation of DMPC-ether/DHPC-ether bicelle

samples [34]. We have found that the peptide order parameter is essentially unchanged between DMPC-ether/DHPC-ether bicelles at 42 °C and bilayer plate samples at 50 °C [16].

Combinations of ^{2}H quadrupolar splittings and ^{15}N/^{1}H dipolar coupling frequencies, individually or together, and in some cases along with ^{15}N chemical shift values, were used to calculate the orientations of peptide helices in the lipid bilayers, using methods described previously [16,22]. Helix tilt τ is the angle between the helix axis and the bilayer normal [10]. We have defined helix azimuthal rotation ρ by first placing Cα of residue one on the x-axis (N-terminal up, positive z direction, with the helix centered at (x=0, y=0)), and then rotating counterclockwise by ρ degrees before tilting toward the x-axis (see Figure 1 of ref. [10]). The net effect is to tilt toward a residue that is located in the first half of the sequence and $-\rho°$ from G^{1} around the helical wheel. Naturally, the C-terminal will swivel oppositely to the N-terminal during tilting. Data uncertainty was estimated to be within ±0.5 kHz based on duplicate samples and measurements using different orientations of glass slide samples [16]. We performed calculations both with a semi-static model and with a more dynamic model that incorporates Gaussian distributions for the helix tilt and azimuthal rotation [35]. The detailed strategy for combined ^{2}H and ^{15}N/^{1}H analysis has been described [16].

Small lipid vesicles incorporating 125 μM peptide and 7.5 mM lipid (1/60) were prepared for CD spectroscopy by sonication. Ten scans were recorded and averaged on a Jasco (Easton, MD) J710 CD spectropolarimeter, using a 1 mm cell path length, 1.0 nm bandwidth, 0.1 nm slit and a scan speed of 20 nm/min. Vesicle solutions with 1/60 peptide/lipid for fluorescence experiments were prepared by dilution, 1/20 with water, of the samples prepared previously for CD spectroscopy. Samples were excited at 280 nm or 295 nm with a 5 nm excitation slit, and emission spectra were recorded between 300 and 420 nm with a 5 nm emission slit using a Hitachi F-2500 fluorescence spectrophotometer. The tyrosine fluorescence contribution is negligible when the excitation wavelength is 295 nm (Figure S4 of the Supporting Information). The spectra from five to ten scans were averaged.

3. RESULTS

The designed model peptides (Table 1, Figure 1) were synthesized successfully, and their identities and levels of purity (> 95%) were confirmed by mass spectrometry and reversed-phase chromatography (Figures S1 and S2 of the Supporting Information). With the hydrophobic core of GWALP-like peptides consisting entirely of residues with a propensity for α-helix formation (Leu-Ala), a predominantly α-helix secondary structure is expected for the bilayer-incorporated peptides and was confirmed by CD spectra (Figure S5 of the Supporting Information) that are similar to those observed for native GWALP23.[22]

By using solid-state NMR methods and aligned samples of peptides incorporated within hydrated lipid-bilayer membranes, it is possible to deduce each peptide's average orientation and describe its dynamic properties, with respect to the lipid bilayer. Oriented glass plate samples were first analyzed by ^{31}P NMR spectroscopy to confirm the alignment of the lipid bilayers. All of the peptide-lipid systems were found to be well-aligned as bilayers, with the appropriate dominant ^{31}P resonances observed for $\beta = 90°$ as well as $\beta = 0°$ macro-alignment (with minimal amounts of unoriented material sometimes seen in the spectra recorded with $\beta = 0°$) (Figure S3 of the Supporting Information).

Initial visual comparisons of ^{2}H NMR quadrupolar splittings (from labeled alanines) of Y^{19}GW^{5} ALP23 and GY^{5,19} ALP23 peptides suggest similarities to those of previous GWALP-like peptides in DLPC, DMPC and DOPC bilayers (Figure 2). This qualitative assessment indicates that the new peptides are indeed helical and moreover may adopt similar orientations to those of GWALP23 and Y^{5}GWALP23, each of which exhibits a similar and

progressively increasing tilt angle with respect to the extent of peptide:lipid hydrophobic mismatch. The sets of ^{2}H quadrupolar splittings for the six labeled alanines, two in each of three independently synthesized samples, in the core helix of each peptide, indeed are similar to those of Y^{5}GWALP23 (Table 2; Figures S6–S7 of the Supporting Information). Because descriptions of the peptide dynamics may vary, depending upon numbers of observables and of fitted parameters [16,35,36], we employed several methods to analyze the peptide orientations and dynamics. The observed ^{2}H quadrupolar splittings were analyzed first by means of a semi-static GALA method [10,16] using a grid search to screen for the lowest RMSD values using helix tilt τ, helix azimuthal rotation ρ, and a principal order parameter S_{zz} as variables.

The results of semi-static GALA analysis (Table 3, Figure 3) reveal similar magnitudes of the tilt angle τ for the Y^{19}, Y^{5}, and Y^{5,19} cousins of GWALP23 in each respective lipid, along with a similar scaling of τ with respect to hydrophobic mismatch, as observed for GWALP23 itself [12]. Regardless of the detailed helix dynamics, the similar helix properties in light of the different Tyr/Trp substitutions are apparent. It is conspicuously apparent that not one of these peptides exhibits the highly extensive dynamic averaging shown by Y^{4,5}GWALP23 [22]. Minimal tilts of ~5° in the longer DOPC lipid were deduced, followed by median tilts of ~10° in DMPC, and larger tilts of ~20° in the shorter DLPC bilayers where greater hydrophobic mismatch occurs. While the tilt angles are similar, it can be inferred from the phase shift in the quadrupolar wave plots that there is a small yet consistent change in the helix azimuthal rotation ρ for Y^{19}GWALP23. While it was previously seen that the W5Y mutation of GWALP23 results in a ~ 10° change in rotation in all tested lipids [22], in contrast a W19Y mutation leads to a rotational shift of similar magnitude in the opposite direction. Furthermore, when the identities of both anchors are changed from Trp to Tyr in GY^{5,19}ALP23, the contributing tyrosine-induced changes appear to cancel each other, such that the final helix rotation does not differ significantly from that of native GWALP23. Figure 5 illustrates the aromatic anchor dependence of ρ in DLPC; and similar trends in ρ were exhibited in all lipids tested (Supplemental Figure S8 of the Supporting Information). These trends do not depend upon the choice of method for treating the dynamics, as the trends for ρ hold also when a Gaussian treatment of the peptide dynamics is applied (see below, and Figure S9 of the Supporting Information).

^{15}N-based SAMPI4 experiments were conducted with Y^{19}GWALP23 in magnetically aligned DMPC-ether/DHPC-ether bicelles (3.2:1 mol:mol). (The ether lipids provide added chemical stability by precluding hydrolysis of the more labile ester bond.) The comparisons with stacked bilayer samples are appropriate because (a) the bicelles and aligned bilayer samples give similar solid-state NMR observables [16], and furthermore (b) peptide helices dispersed in ether and ester lipids also give similar solid-state NMR observables that indicate similar Trp orientations and dynamics [23]. For the SAMPI4 experiments, Y^{19}GWALP23 was labeled with ^{15}N in the Leu-Ala core residues 13 through 17. The observed “PISA” wheel pattern of the resonances is nearly centered on that from previous Y^{5}GWALP23 spectra, but with a somewhat tighter wheel pattern (Figure 6). The ^{15}N chemical shifts span a range of 89–98.3 ppm (Table 4), which is smaller than the range of 84–101 ppm observed in previous spectra for GWALP23 or Y^{5}GWALP23 [22]. The ^{15}N/^{1}H dipolar coupling frequencies also span a slightly diminished range, (Table 4).

With an increased number of NMR observables for Y^{19}GWALP23 in DMPC, we were able to employ a combined analysis of available data that used a Gaussian treatment of peptide dynamics, for comparison with a semi-static method [15,16]. Using quadrupolar splittings of six ^{2}H-Ala methyl groups, along with the ^{15}N chemical shift frequencies and ^{15}N/^{1}H dipolar coupling frequencies of five core residues, the analysis of 16 restraints produced a well fitting solution with low RMSD (1.1 kHz) (Figure 7C). As seen in the quadrupolar and dipolar wave plots (Figure 7A and 7B), independent measurements agree on an orientation wherein τ_{o} is

about 24° and ρ_o is 321° (Table 5). It has been well established that a semi-static analysis underestimates τ_o by up to 20° for highly dynamic transmembrane helices [16,37,38] and by up to 10° for cases of intermediate dynamics, including GWALP23, that show intermediate values of σ_ρ, namely ~50°−60° [16,36] This trend is seen to continue for Y^5 GWALP23 and Y^{19}GWALP23 (Tables 3, 5). Importantly, the trends are remarkably consistent, such that the comparisons among related peptide/lipid systems remain valid when identical treatments for the dynamics are employed[16] Indeed, comparisons (differences) in tilt, or dynamics, when the lipid identity or an aspect of the peptide helix is changed arguably are more meaningful than is the absolute magnitude of tilt based on a single analysis. The uncertainties in τ_o and ρ_o will depend upon the particular method of analysis, the fit for σ_ρ and the number of fitted parameters. The uncertainties in the solid-state NMR observables are in the range of 0.5–1.0 kHz. As a test of the confidence levels, we examined the consequences of introducing systematic errors into the NMR data (see [16,36]). For the semi-static analysis, when all of the ^{2}H quadrupolar splittings are offset by ±2 kHz, we find that the deduced ρ_o changes by less than 1° and the deduced τ_o by less than 0.6°.

Interestingly, and in agreement with previous findings [16,36–38], the trends in ρ_o among GWALP23, Y^5 GWALP23 and Y^{19}GWALP23 are independent (Table 5) of the method that is used for analyzing the dynamics. Furthermore, when the Gaussian analysis is employed, similar values of σ_ρ are observed for the three peptide helices (see also Figure S9 of the Supporting Information). As seen in Figure 7D, Y^{19}GWALP23 exhibits similar dynamics to GWALP23 and Y^5 GWALP23 in DMPC, reflected also in the similar fits for σ_τ and σ_ρ (Table 5), although σ_ρ appears marginally larger. Notably, each of these peptides exhibits *much less* dynamic averaging of the solid-state NMR observables than does the highly dynamic $Y^{4,5}$, GWALP23[22]

Steady-state fluorescence experiments with Y^{19}GWALP23 in DOPC vesicles reveal a slightly less polar environment for the remaining single Trp residue when its location is N-terminal to the core helix. Indeed, the entire spectrum for Y^{19}GWALP23 in DOPC is blue-shifted by about 3 nm, compared to the spectrum for Y^5GWALP23 in DOPC (Figure 8). The environment surrounding W^5 is therefore less polar than the environment surrounding W^{19}. Translation as well as rotation of the tilted bilayer-spanning helix will influence the respective local environments of W^5 and W^{19}.

4. DISCUSSION

Direct comparisons between the properties conferred by interfacial Tyr and Trp residues are important because, while each of these aromatic residues favors an interfacial location, with hydrogen bonding, they nevertheless may bestow different functional outcomes, for example different channel lifetimes and different cation conductances for gramicidin channels [21]. Furthermore, the average trans-bilayer Trp ring depth differs by about 3–4 Å from the average Tyr ring location (ensemble average from 460 integral membrane proteins), with Tyr rings occupying interfacial positions at the hydrophobic boundary and Trp rings occupying "midpolar" positions somewhat closer to the bilayer center [39]. In this context, it is important to characterize the influence, if any, of individual Trp-to-Tyr substitutions for the properties of defined membrane-spanning helices.

GWALP23 is a favorable host framework for these types of single-residue exchanges because this parent ("host") transmembrane peptide exhibits only modest averaging of the solid-state NMR observables [12,15,16,40]. An initial comparison of Trp versus Tyr anchoring properties was accomplished at position 5 near the N-terminus of GWALP23, where the two aromatic residues were found to behave quite similarly [22]. We have further analyzed the system by comparing N-terminal (position 5) and C-terminal (position 19) Trp and Tyr residues in GWALP23.

The ^{2}H quadrupolar wave plots observed for Y^{19}GWALP23 and GY^{5,19}ALP23 are similar to those observed previously for GWALP23 itself as well as Y^{5}GWALP23 [22], which is suggestive of similar transmembrane orientations and dynamics for each peptide. Indeed, the GALA analysis of the ^{2}H quadrupolar splittings, with a principal order parameter S_{zz}, indicates similar magnitudes of tilt for Y^{19}GWALP23, Y^{5}GWALP23, GY^{5,19}ALP23, and GWALP23 in each lipid membrane that was examined. The relative tilt magnitudes for each peptide furthermore adapt systematically based on the extent of peptide/lipid hydrophobic mismatch in DLPC, DMPC or DOPC bilayer membranes, with greater tilt observed in thinner bilayers. The systematic trend for changing the tilt in bilayers of different thickness is independent of the method of analysis. Similar to observations with GWALP23 itself, the trends illustrate that each of these peptides is less dynamic than those that possess more than two interfacial aromatic residues, such as WALP23 [41], WWALP23 [16], WLP23 [40] and Y^{4,5}GWALP23 [22].

Though the Tyr-19 anchored peptides are less dynamic than transmembrane peptides that possess more than two interfacial Trp or Tyr residues, it would appear they are nevertheless slightly more dynamic than GWALP23 or Y^{5}GWALP23. The results suggest that residue W19 may be critical for achieving the lower limit of dynamic averaging within this series.
The ^{15}N-based SAMPI4 experiments suggest the increased dynamic averaging, evidenced from the reduced diameter for the PISA-wheel of Y^{19}GWALP23 (Figure 6). With WWALP23 and WLP23, each having four Trp residues, though the helices are tilted, the ^{15}N resonances in the respective PISA wheels collapse to a single point of overlapping resonances [16,40]. Indeed, the PISA wheel for Y^{19}GWALP23 is only slightly smaller than that of Y^{5}GWALP23 and much larger than the collapsed wheels that are observed for WWALP23[16] and WLP23[40] . The similar amplitudes of the Gaussian probability curves for ρ (see below, and Figure S9 of the Supporting Information) furthermore illustrate similar extents of dynamic averaging for Y^{19}GWALP23 and GY^{5,19} ALP23 as well as Y^{5} GWALP23.

We sought to compare also the semi-static and Gaussian dynamic treatments of the more extensive sets of solid-state NMR observables for Y^{19}GWALP23 in DMPC. A combined method of analysis for ^{2}N and ^{2}H data sets was recently described in detail[16] and has been applied also to Y^{5} GWALP23[22] . Compared to Y^{5} GWALP23, Y^{19}GWALP23 displays a similar tilt magnitude τ_0, with a similar σ_τ (Table 5) and a slightly larger σ_ρ (Table 5). Notably, the σ_τ values are small for the entire set of GWALP23, Y^{19}GWALP23 and Y^{5} GWALP23; and the σ_ρ values are in the moderate range. While we remain cautious about applying the Gaussian analysis for small data sets, we nevertheless attempted to estimate possible ranges for σ_τ and σ_ρ from coarse Gaussian treatments of the sets of ^{2}H quadrupolar splittings for peptides in DLPC and DOPC (Table S1 of the Supporting Information). These estimates suggest that σ_ρ remains in the moderate range for GWALP23, Y^{19}GWALP23 and Y^{5} GWALP23 in DLPC and DOPC. Importantly, the noted trends for ρ_o, with respect to aromatic residue identity as well as host lipid identity (see below), are preserved even for the coarse estimates in Table S1.

Steady-state fluorescence emission spectra of WALP and GWALP peptides reflect the summed emissions from multiple Trp fluorophores. The single-Trp Y^{5} GWALP23 and Y^{19}GWALP23 peptides, by contrast, possess only a single fluorescence reporter and potentially could provide more quantitative information about the local environment of the remaining Trp indole ring. Indeed a blue shift of ~3 nm is observed for W5 compared to W19, across the entire emission spectrum (Figure 8). The spectral results are consistent with our understanding of the helix tilting in the bilayer. Given that GWALP23 tilts in the direction of W5 (with W19 being radially offset by only 40°), W5 becomes further submerged into the bilayer, while at the same time W19 in the tilted helix is more exposed to the aqueous phase. Helix translation with respect to the bilayer center also could contribute to the observed changes in fluorescence λ_{max}. Indeed, a translation of 3 Å has been modeled, along with tilting and bilayer deformation, to explain

the accommodation of the single charge in GWALP23-R14[42] . When single tyrosines are introduced, the fluorescence emission spectra of $Y^{19}GW^{5}$ ALP23 and $Y^{5}GW^{19}$ ALP23 are in accord with the tilted orientation of GWALP23.

The identities and locations of the interfacial aromatic residues govern the azimuthal rotation of the transmembrane helix (in the absence of charged residues, as is the case here). Actually , in lipid-bilayer environments that range from DOPC to DMPC to DLPC, each peptide within the family exhibits a unique preference for its azimuthal rotation, demonstrating specific preferences that relate to the anchor group identity (W or Y) and location (position 5 or 19). It was previously seen that replacement of W5 with Y5 in GWALP23 produced a shift of ~10° in the azimuthal rotation. The present experiments show that a change from W19 to Y19 shifts ρ_o by a similar magnitude but in the opposite direction. Interestingly, the $W^{5}Y^{19}$ and $Y^{5}W^{19}$ peptides differ ~20° in their rotational preference, and residues 5 and 19 project 40° apart on a helical wheel. When both Y^{5} and Y^{19} are present, the rotational preference matches that for GWALP23, with W^{5} and W^{19} present (Table 3). As a caveat, these rotational priorities are altered if even one charged residue is present in a rather central location[26]

We note also that the azimuthal rotation preference changes systematically with the identity and thickness of the host lipid (Table 3) while, as noted above, the differences with respect to anchor group identity (W or Y) and location (position 5 or 19) remain similar in each of the lipids. It has furthermore been suggested that the lipid thickness, helix geometry and immersion depths of individual residues impose constraints for the rotation preferences [43].

One can imagine a scenario in which each interfacial aromatic residue is independently trying to influence the helix orientation and thereby best position itself with respect to the lipid head groups and aqueous interface, so as to enhance its own hydrogen bonding capabilities. A resulting competition could lead to the dynamic averaging observed with previous WALP peptides that have multiple aromatic groups, each attempting to achieve a favorable location at the bilayer interface. These substantial variations in helix dynamics with respect to aromatic ring arrangements in turn could modulate the functional activities and signaling performed by membrane proteins.

Within such a scenario of ongoing aromatic ring competition, it is known also that the Trp side chain does possess rotational freedom to adapt to a given environment and produce a favorable orientation of the indole ring [23]. In a bilayer, the C-terminal Trp of any transmembrane peptide is expected to adjust its side-chain $\chi1$ and $\chi2$ torsion angles so as to "flip" the indole ring with respect to the local side-chain orientation observed at the N-terminal, in order to reorient the indole amino moiety toward the aqueous phase. This indole reorientation has in fact been observed both for WALP peptides [23] and for ^{2}H-labled Trp residues in GWALP23 [15]. It was also seen that as the GWALP23 helix adopted different orientations in different bilayers, the indole rings themselves adjusted somewhat independently of the helix to achieve optimal ring placement [15]. The asymmetry of the C-terminal versus N-terminal aromatic residue placement in a transmembrane helix may be manifest in a physiological context. For example, Type 1 single-span membrane helices show a preference for Tyr at the C-terminal [18]. Additionally, further statistical analysis that also included polytopic proteins (those with multiple membrane-spanning helices) showed a small preference for Trp on the non-cytoplasmic side [20].

It is interesting that when both GWALP23 tryptophans are replaced with tyrosine, the peptide helix adopts a nearly identical orientation. It would thus appear that the net residue contributions cancel out and that the radial placement of the aromatic residues is a predominant factor. Indeed, it was recently shown that the azimuthal rotation changes systematically as the radial positions of Trp residues are varied in pair-wise fashion within GWALP23 [15]. While the chief rotation determinants, in the absence of charged residues, are the positions of single

aromatic residues at each interface, Trp and Tyr differ by about 10° in their preferences for the helix rotation, such that the identities of the aromatic residues play a modest yet important role.

In summary, the identities, placements and importantly the total number of amphipathic aromatic residues are important factors in determining the preferred orientations and dynamics of transmembrane peptides within lipid bilayer membranes. The choice of Trp versus Tyr is less important than the radial positions of the aromatic residues around the helix axis. Helix asymmetry is manifest in the observation that W5 of Y^{19}GWALP23 is more deeply submerged into the bilayer than is W19 of Y^{5}GWALP23, due to the particular location and tilted orientation of the membrane-spanning helix. “Too many” aromatic rings (more than one N-terminal and one C-terminal) cause extensive dynamic averaging. When Trp is absent, the orientation and dynamics of $GY^{5, 19}$ALP23 are nevertheless similar to the properties of GWALP23, and the extent of dynamic averaging is much less than when three aromatic rings are present in $Y^{4,5}$GWALP23. The fundamental features observed for these model systems represent portions of a larger set of molecular interactions that govern the functioning of membrane proteins.

Supplementary Material

Refer to Web version on PubMed Central for supplementary material.

Acknowledgments

We thank Vitaly Vostrikov and Johanna Rankenberg for helpful discussions.

ABBREVIATIONS and FOOTNOTES

CD	circular dichroism
DLPC	1,2-dilauroylphosphatidylcholine
DMPC	1,2-dimyristoylphosphatidylcholine
DOPC	1,2-dioleoylphosphatidylcholine
DMPC-ether	1,2-di-O-myristoylphosphatidylcholine
DHPC-ether	1,2-di-O-hexylphosphatidylcholine
Fmoc	Fluorenylmethoxycarbonyl
GALA	Geometric analysis of labeled alanines
GWALP23	acetyl-GGALW$(LA)_6$LWLAGA-[ethanol]amide
MtBE	methyl-*t*-butyl ether
PISEMA	Polarization inversion spin exchange at magic angle
PISA	Polar index slant angles
RMSD	root mean squared deviation
TFA	trifluoroacetic acid
WWALP23	acetyl-GWALW$(LA)_6$LWLAWA-[ethanol]amide

REFERENCES

1. Luo W, Cady SD, Hong M. Immobilization of the influenza A M2 transmembrane peptide in virus envelope-mimetic lipid membranes: a solid-state NMR investigation. Biochemistry. 2009; 48:6361–6368. [PubMed: 19489611]
2. Carruthers A, Melchior DL. Human erythrocyte hexose transporter activity is governed by bilayer lipid composition in reconstituted vesicles. Biochemistry. 1984; 23:6901–6911. [PubMed: 6543323]
3. Brown MF. Modulation of rhodopsin function by properties of the membrane bilayer. Chem Phys Lipids. 1994; 73:159–180. [PubMed: 8001180]
4. Cybulski LE, Martin M, Mansilla MC, Fernandez A, de Mendoza D. Membrane thickness cue for cold sensing in a bacterium. Curr Biol. 2010; 20:1539–1544. [PubMed: 20705470]
5. Montecucco C, Smith GA, Dabbeni-sala F, Johannsson A, Galante YM, Bisson R. Bilayer thickness and enzymatic activity in the mitochondrial cytochrome c oxidase and ATPase complex. FEBS Lett. 1982; 144:145–148. [PubMed: 6286354]
6. Hong H, Tamm LK. Elastic coupling of integral membrane protein stability to lipid bilayer forces. Proc Natl Acad Sci U S A. 2004; 101:4065–4070. [PubMed: 14990786]
7. Yang FY, Hwang F. Effect of non-bilayer lipids on the activity of membrane enzymes. Chem Phys Lipids. 1996; 81:197–202.
8. Moe P, Bloe Blount P. Assessment of potential stimuli for mechano-dependent gating of MscL: effects of pressure, tension, and lipid headgroups. Biochemistry. 2005; 44:12239–12244. [PubMed: 16142922]
9. Killian JA, Salemink I, de Planque MR, Lindblom G, Koeppe RE, II; Greathouse DV. Induction of nonbilayer structures in diacylphosphatidylcholine model membranes by transmembrane alpha-helical peptides: importance of hydrophobic mismatch and proposed role of tryptophans. Biochemistry. 1996; 35:1037–1045. [PubMed: 8547239]
10. van der Wel PC, Strandberg E, Killian JA, Koeppe RE II. Geometry and intrinsic tilt of a tryptophan-anchored transmembrane alpha-helix determined by ^{2}H NMR. Biophys J. 2002; 83:1479–1488. [PubMed: 12202373]
11. Vostrikov VV, Grant CV, Daily AE, Opella SJ, Koeppe RE II. Comparison of "Polarization inversion with spin exchange at magic angle" and "geometric analysis of labeled alanines" methods for transmembrane helix alignment. J Am Chem Soc. 2008; 130:12584–12585. [PubMed: 18763771]
12. Vostrikov VV, Daily AE, Greathouse DV, Koeppe RE II. Charged or aromatic anchor residue dependence of transmembrane peptide tilt. J Biol Chem. 2010; 285:31723–31730. [PubMed: 20667827]
13. De Planque MRR, Kruijtzer JA, Liskamp RM, Marsh D, Greathouse DV, Koeppe RE II, de Kruijff B, Killian JA. Different membrane anchoring positions of tryptophan and lysine in synthetic transmembrane alpha-helical peptides. J. Biol. Chem. 1999; 274:20839–20846. [PubMed: 10409625]
14. de Planque MR, Boots JW, Rijkers DT, Liskamp RM, Greathouse DV, Killian JA. The effects of hydrophobic mismatch between phosphatidylcholine bilayers and transmembrane alpha-helical peptides depend on the nature of interfacially exposed aromatic and charged residues. Biochemistry. 2002; 41:8396–8404. [PubMed: 12081488]
15. Vostrikov VV, Koeppe RE II. Response of GWALP transmembrane peptides to changes in the tryptophan anchor positions. Biochemistry. 2011; 50:7522–7535. [PubMed: 21800919]
16. Vostrikov VV, Grant CV, Opella SJ, Koeppe RE II. On the combined analysis of ^{2}H and ^{15}N/^{1}H solid-state NMR data for determination of transmembrane peptide orientation and dynamics. Biophys J. 2011; 101:2939–2947. [PubMed: 22208192]
17. de Planque MR, Bonev BB, Demmers JA, Greathouse DV, Koeppe RE II, Separovic F, Watts A, Killian JA. Interfacial anchor properties of tryptophan residues in transmembrane peptides can dominate over hydrophobic matching effects in peptide-lipid interactions. Biochemistry. 2003; 42:5341–5348. [PubMed: 12731875]
18. Landolt-Marticorena C, Williams KA, Deber CM, Reithmeier RA. Non-random distribution of amino acids in the transmembrane segments of human type I single span membrane proteins. J Mol Biol. 1993; 229:602–608. [PubMed: 8433362]

19. Arkin IT, Brunger AT. Statistical analysis of predicted transmembrane alpha-helices. Biochim Biophys Acta. 1998; 1429:113–128. [PubMed: 9920390]
20. Ulmschneider MB, Sansom MS. Amino acid distributions in integral membrane protein structures. Biochim Biophys Acta. 2001; 1512:1–14. [PubMed: 11334619]
21. Fonseca V, Daumas P, Ranjalahy-Rasoloarijao L, Heitz F, Lazaro R, Trudelle Y, Andersen OS. Gramicidin channels that have no tryptophan residues. Biochemistry. 1992; 31:5340–5350. [PubMed: 1376621]
22. Gleason NJ, Vostrikov VV, Greathouse DV, Grant CV, Opella SJ, Koeppe RE II. Tyrosine replacing tryptophan as an anchor in GWALP peptides. Biochemistry. 2012; 51:2044–2053. [PubMed: 22364236]
23. van der Wel PC, Reed ND, Greathouse DV, Koeppe RE II. Orientation and motion of tryptophan interfacial anchors in membrane-spanning peptides. Biochemistry. 2007; 46:7514–7524. [PubMed: 17530863]
24. Thomas R, Vostrikov VV, Greathouse DV, Koeppe RE II. Influence of proline upon the folding and geometry of the WALP19 transmembrane peptide. Biochemistry. 2009; 48:11883–11891. [PubMed: 19891499]
25. Siegel DP, Cherezov V, Greathouse DV, Koeppe RE II, Killian JA, Caffrey M. Transmembrane peptides stabilize inverted cubic phases in a biphasic lengthdependent manner: Implications for protein-induced membrane fusion. Biophys. J. 2006; 90:200–211. [PubMed: 16214859]
26. Vostrikov VV, Hall BA, Sansom MSP, Koeppe RE II. Accommodation of a Central Arginine in a Transmembrane Peptide by Changing the Placement of Anchor Residues. J. Phys. Chem. B. 2012; 116:12980–12990. [PubMed: 23030363]
27. van der Wel PC, Strandberg E, Killian JA, Koeppe REn. Geometry and intrinsic tilt of a tryptophan-anchored transmembrane alpha-helix determined by ^{2}H NMR. Biophys J. 2002; 83:1479–1488. [PubMed: 12202373]
28. Davis JH, Jeffrey KR, Bloom M, Valic MI, Higgs TP. Quadrupolar echo deuteron magnetic resonance spectroscopy in ordered hydrocarbon chains. Chem. Phys. Lett. 1976; 42:390–394.
29. Opella SJ, Marassi FM. Structure determination of membrane proteins by NMR spectroscopy. Chem. Rev. 2004; 104:3587–3606. [PubMed: 15303829]
30. Marassi FM, Opella SJ. A solid-state NMR index of helical membrane protein structure and topology. J Magn Reson. 2000; 144:150–155. [PubMed: 10783285]
31. Wu CH, Ramamoorthy A, Opella SJ. High-Resolution Heteronuclear Dipolar Solid-State NMR Spectroscopy. J. Magn. Reson. Ser. 1994; 109:270–272.
32. Nevzorov AA, Opella SJ. A "magic sandwich" pulse sequence with reduced offset dependence for high-resolution separated local field spectroscopy. J Magn Reson. 2003; 164:182–186. [PubMed: 12932472]
33. Cook GA, Opella SJ. NMR studies of p7 protein from hepatitis C virus. Eur. Biophys. J. 2010; 39:1097–1104. [PubMed: 19727701]
34. Triba MN, Warschawski DE, Devaux PF. Reinvestigation by phosphorus NMR of lipid distribution in bicelles. Biophys J. 2005; 88:1887–1901. [PubMed: 15626702]
35. Strandberg E, Esteban-Martin S, Salgado J, Ulrich AS. Orientation and dynamics of peptides in membranes calculated from ^{2}H-NMR data. Biophys J. 2009; 96:3223–3232. [PubMed: 19383466]
36. Strandberg E, Esteban-Martin S, Ulrich AS, Salgado J. Hydrophobic mismatch of mobile transmembrane helices: Merging theory and experiments. Biochim. Biophys. Acta. 2012; 1818:1242–1249. [PubMed: 22326890]
37. Esteban-Martín S, Salgado J. The dynamic orientation of membrane-bound peptides: bridging simulations and experiments. Biophys. J. 2007; 93:4278–4288. [PubMed: 17720729]
38. Holt A, Rougier L, Reat V, Jolibois F, Saurel O, Czaplicki J, Killian JA, Milon A. Order Parameters of a Transmembrane Helix in a Fluid Bilayer: Case Study of a WALP Peptide. Biophys. J. 2010; 98:1864–1872. [PubMed: 20441750]
39. Pogozheva ID, Tristram-Nagle S, Mosberg HI, Lomize AL. Structural adaptations of proteins to different biological membranes. Biochim. Biophys. Acta Biomembr. 2013; xx in press.

40. Grage SL, Strandberg E, Wadhwani P, Esteban-Martin S, Salgado J, Ulrich AS. Comparative analysis of the orientation of transmembrane peptides using solid-state H-2- and N-15-NMR: mobility matters. Eur. Biophys. J. Biophys. Lett. 2012; 41:475–482.

41. Strandberg E, Ozdirekcan S, Rijkers DT, van der Wel PC, Koeppe RE II, Liskamp RM, Killian JA. Tilt angles of transmembrane model peptides in oriented and non-oriented lipid bilayers as determined by ^{2}H solid-state NMR. Biophys J. 2004; 86:3709–3721. [PubMed: 15189867]

42. Vostrikov VV, Hall BA, Greathouse DV, Koeppe RE II, Sansom MSP. Changes in transmembrane helix alignment by arginine residues revealed by solid-state NMR experiments and coarse-grained MD simulations. J. Am. Chem. Soc. 2010; 132:5803–5811. [PubMed: 20373735]

43. Sánchez-Munoz OL, Strandberg E, Esteban-Martín E, Grage SL, Ulrich AS, Salgado J. Canonical Azimuthal Rotations and Flanking Residues Constrain the Orientation of Transmembrane Helices. Biophys. J. 2013; 104:1508–1516. [PubMed: 23561527]

44. DeLano WL. The PyMOL Molecular Graphics System. 2002

45. Pulay P, Scherer EM, van der Wel PCA, Koeppe RE II. Importance of tensor asymmetry for the analysis of H-2 NMR spectra from deuterated aromatic rings. J. Am. Chem. Soc. 2005; 127:17488–17493. [PubMed: 16332101]

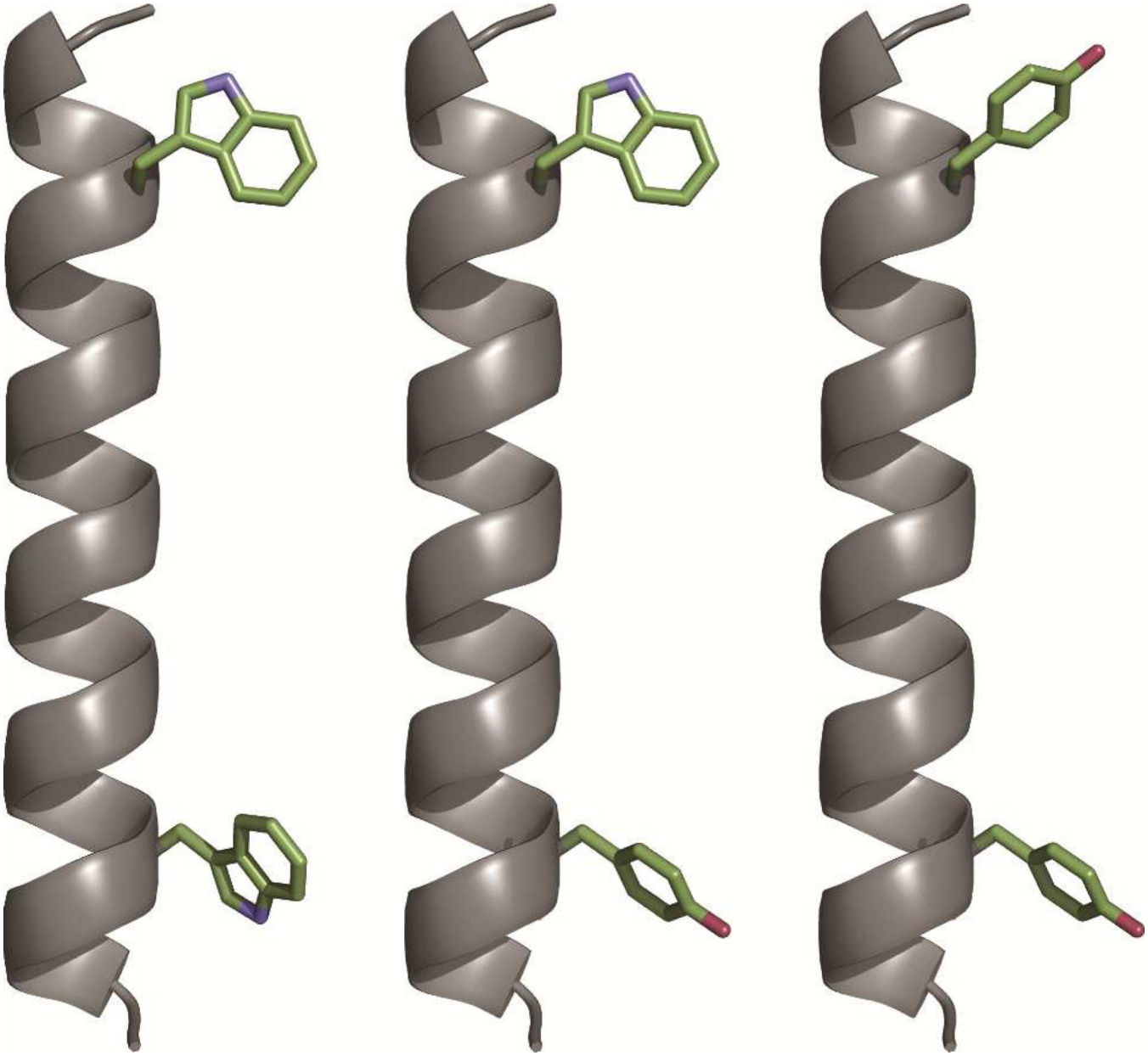

Figure 1.

Representative models of GWALP23, Y^{19}GWALP23 and $Y^{5,19}$GALP23 (left to right), showing the locations of aromatic side chains on a ribbon helix, drawn using PyMOL[44] The side-chain orientations are arbitrary.

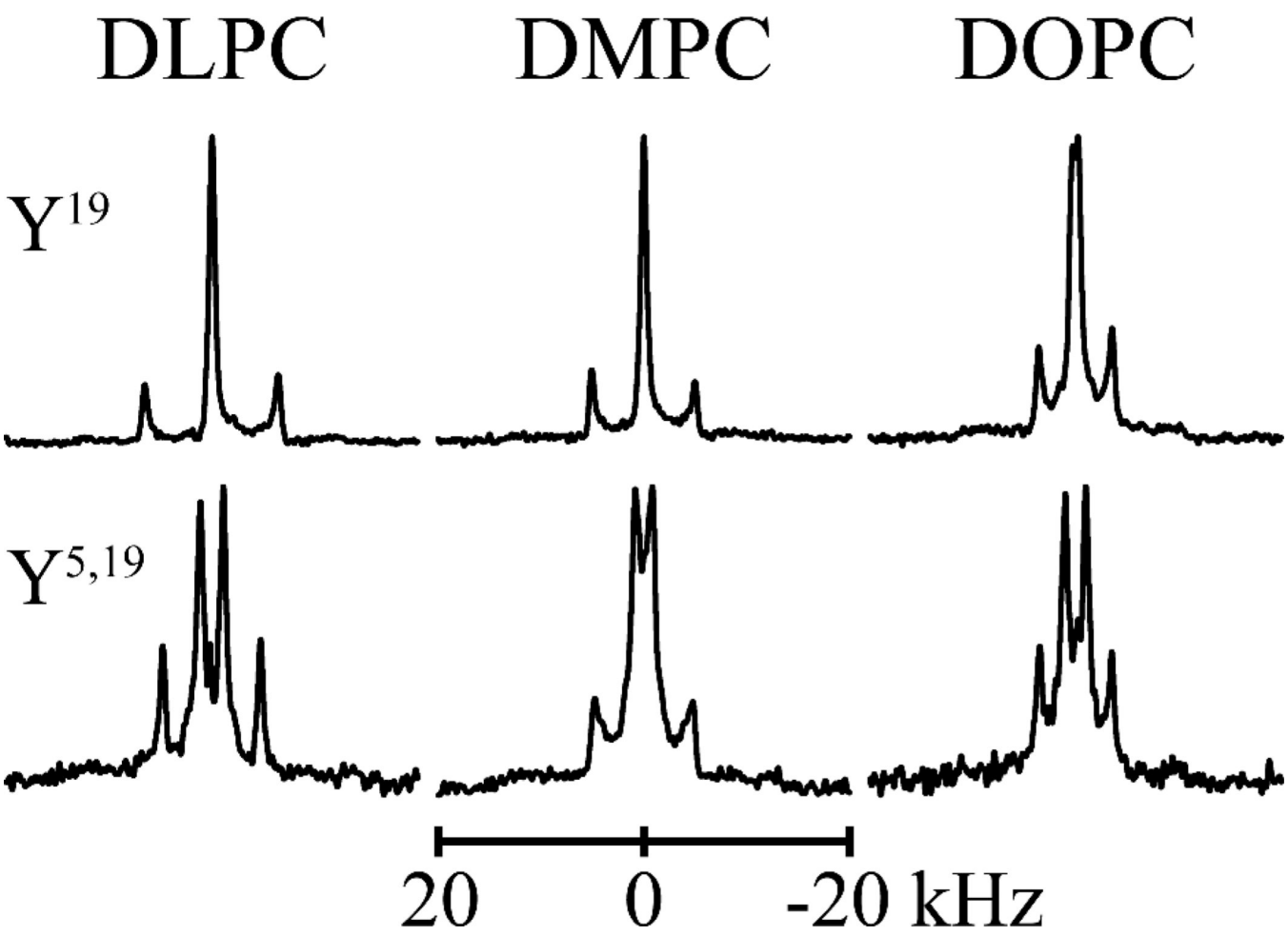

Figure 2.

^{2}H NMR spectra of (top to bottom) Y^{19}GWALP23 and $Y^{5,19}$GALP23, each labeled at Ala^{17} (100% ^{2}H) and Ala^{7} (60% ^{2}H), in hydrated oriented bilayers of DLPC, DMPC and DOPC. Peptide/lipid ratio, 1/60 (mol/mol); 50 °C; β = 90° sample orientation. Complete spectra set of all Ala-d4 labeled peptides are included in Supplemental Figures S6 and S7 of the Supporting Information.

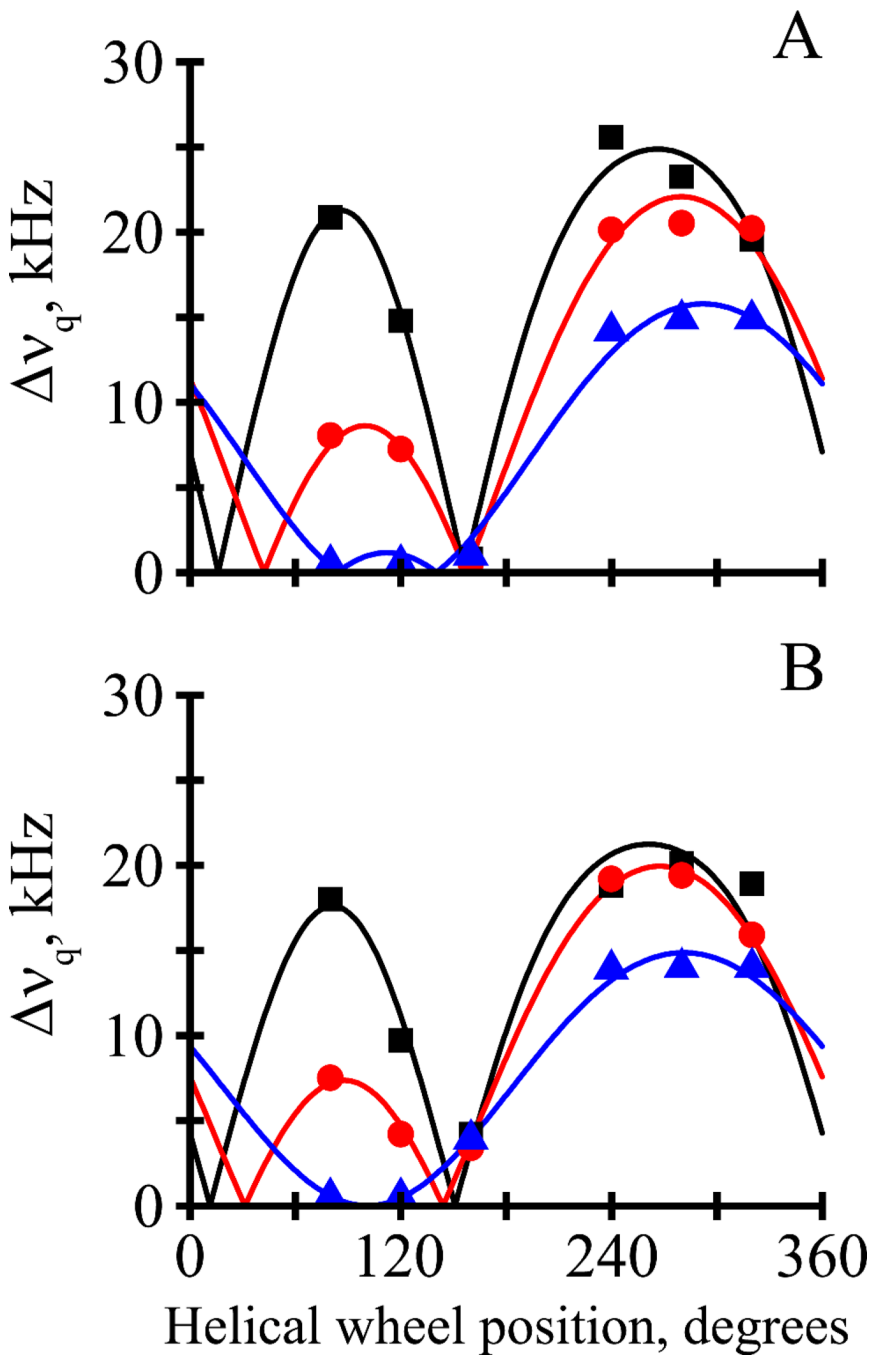

Figure 3.

GALA semi-static analysis of Ala-d4 quadrupolar splittings using variable S_{zz} (see (26)). Quadrupolar wave plots are shown for Y^{19}GWALP23 (A) and $Y^{5,19}$GALP23 (B) in oriented bilayers of DLPC (black squares), DMPC (red circles) and DOPC (blue triangles). Fitted curves represent theoretical $\Delta\nu_q$ values for orientations corresponding to best-fit values of τ and ρ.

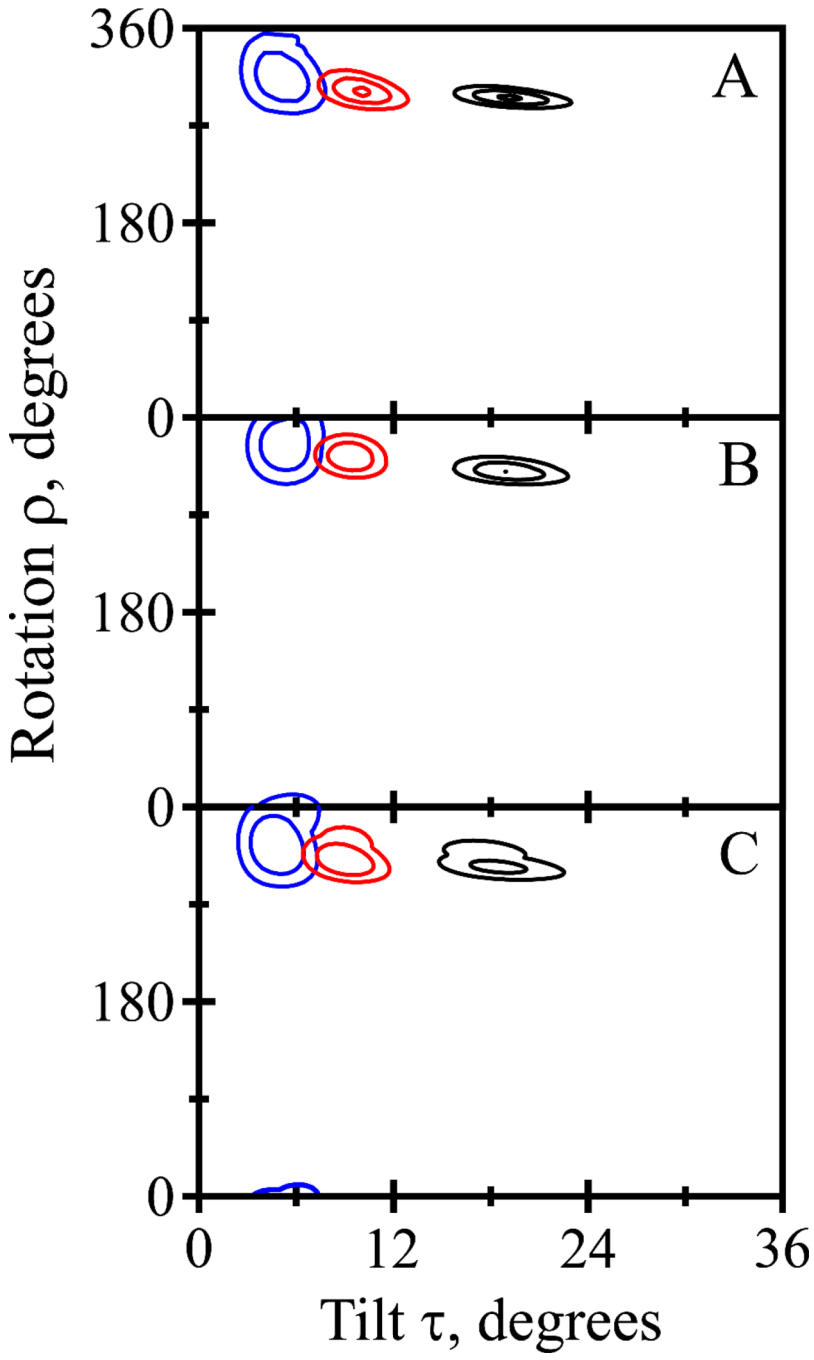

Figure 4.

RMSD contour plots for apparent average tilt τ and rotation ρ resulting from semi-static GALA analysis of Y^{5}GWALP23 (A), Y^{19}GWALP23 (B) and $Y^{5,19}$ GALP23 (C) in DLPC (black), DMPC (red), and DOPC (blue). Contour level increments are 1 kHz, with the outermost contour in each set corresponding to 3 kHz.

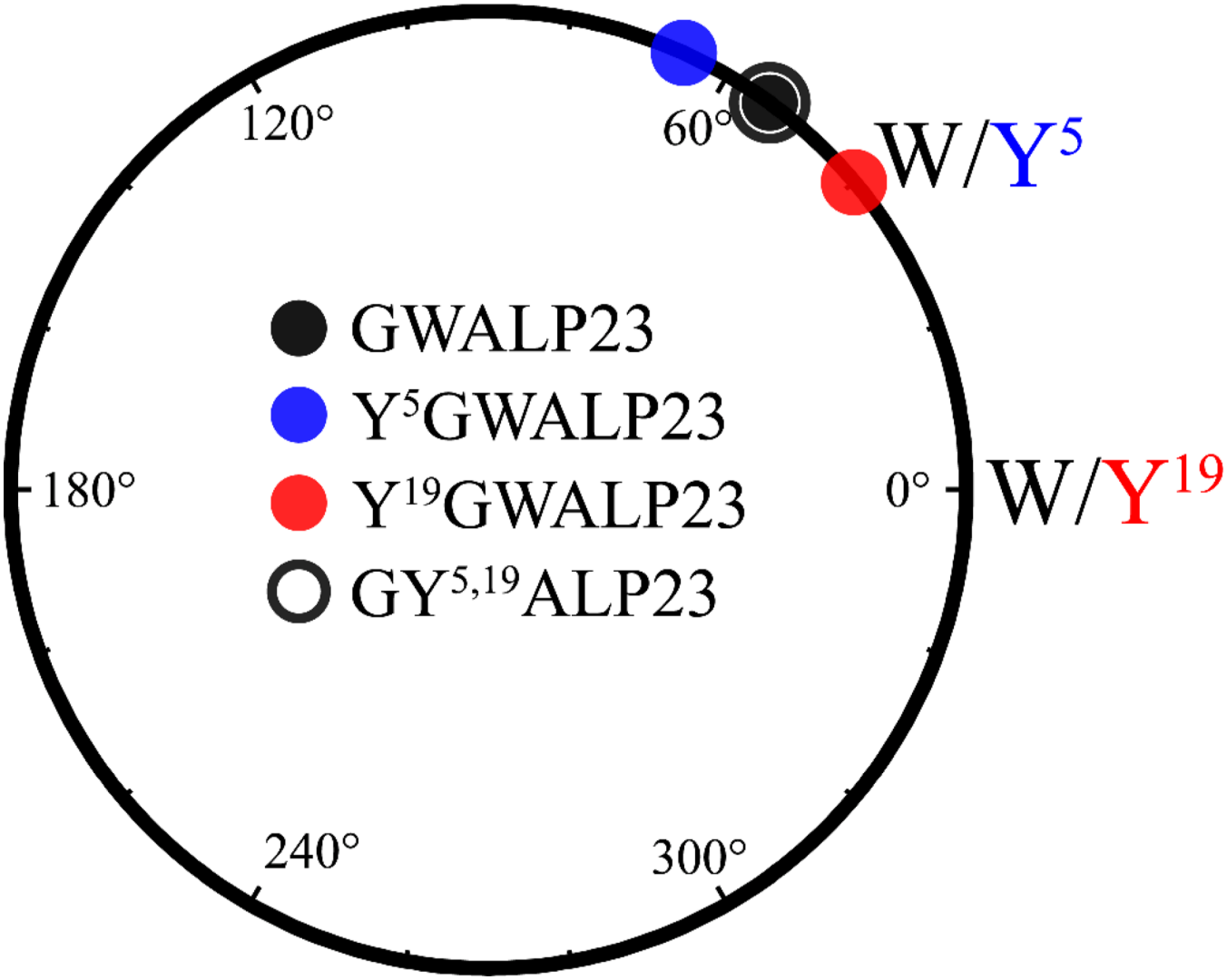

Figure 5.

Helical wheel diagram to illustrate the dependence of the $GX^{5,19}$ ALP23 helix azimuthal rotation angle ρ, in DLPC membranes, on aromatic residue identity. The radial positions of residues 5 and 19 are indicated, as are the preferred ρ values for the W^5W^{19}, Y^5W^{19}, W^5Y^{19}, and Y^5Y^{19} members of the GWALP23 family of peptides.

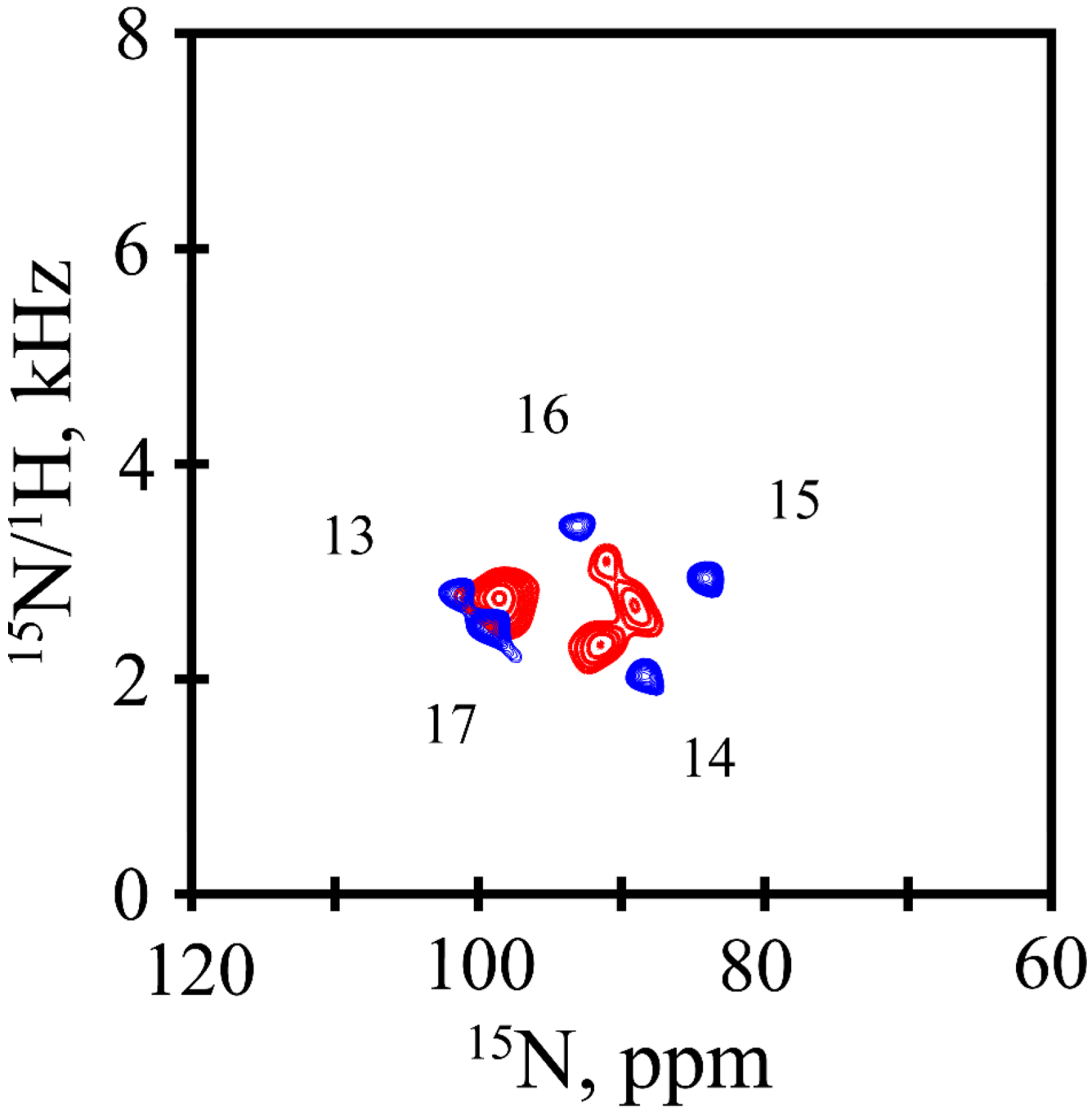

Figure 6.
SAMPI4 spectra, with assignments, for Y^{19}GWALP23 (red) and Y^{5}GWALP23 (blue), each ^{15}N labeled in residues 13–17. Peptide/lipid ratio, 1/80 (mol/mol); 42 °C; bicelles of DMPC-ether/DHPC-ether (q = 3.2).

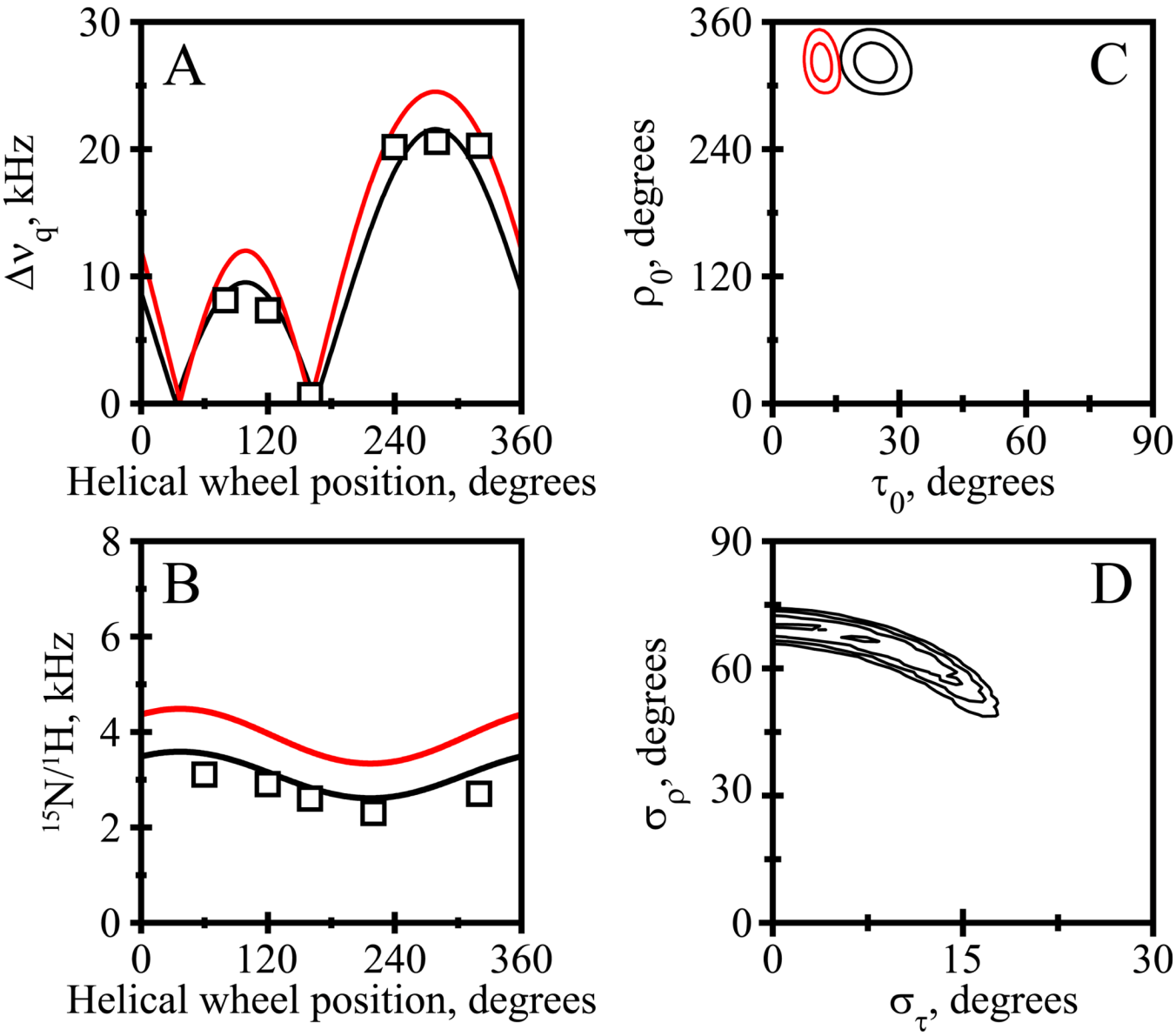

Figure 7.

Combined ^{15}N and ^{2}H analysis for Y^{19}GWALP23 in DMPC. A. Quadrupolar waves from Gaussian dynamics (black curve) and semi-static (red curve) analysis. B. Dipolar waves from Gaussian (black curve) and semi-static (red curve) analysis. C. RMSD (τ_o, ρ_o) graph for the Gaussian (black contours) and semi-static (red contours) analyses, contoured at 2 and 3 kHz. D. RMSD (σ_τ, σ_ρ)graph for the Gaussian dynamics analysis, from 1.10 to 1.19 kHz in 0.03 kHz contours.

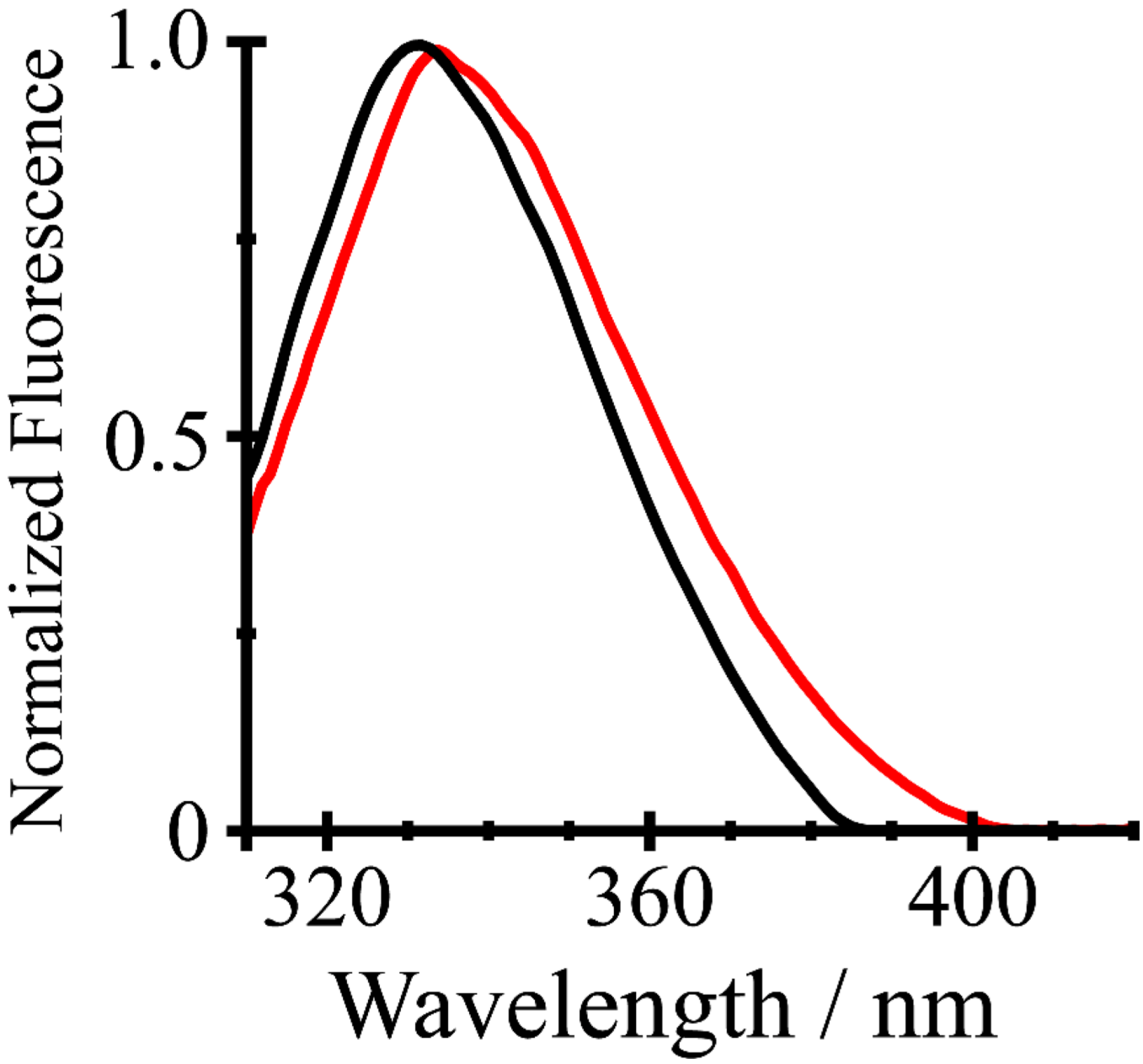

Figure 8.
Steady-state fluorescence spectra of Y^{19}GWALP23 (black) and Y^{5}GWALP23 (red) in DOPC vesicles excited at 295 nm.

Table 1

Sequences of GWALP23-like peptides[a]

Name	Sequence
GWALP23	a-GGALW^{5}LALALALALALALW^{19}LAGA-e
Y^{5}GWALP23	a-GGALY^{5}LALALALALALALW^{19}LAGA-amide
Y^{19}GWALP23	a-GGALW^{5}LALALALALALALY^{19}LAGA-amide
Y^{5,19}GALP23	a-GGALY^{5}LALALALALALALY^{19}LAGA-amide

[a]Abbreviations: “a” denotes “acetyl” and “e” denotes “ethanolamide.”

Table 2

Observed ^{2}H quadrupolar splittings[a] for labeled alanines in Tyr-based analogues of GWALP23 in three lipid bilayers

	DLPC			DMPC			DOPC		
Ala	$b_{\mathbf{Y^5}}$	$\mathbf{Y^{19}}$	$\mathbf{Y^{5,19}}$	$b_{\mathbf{Y^5}}$	$\mathbf{Y^{19}}$	$\mathbf{Y^{5,19}}$	$b_{\mathbf{Y^5}}$	$\mathbf{Y^{19}}$	$\mathbf{Y^{5,19}}$
7	29.3	25.6	18.8	22.8	20.1	19.2	16.2	14.2	13.9
9	24.0	20.9	18.0	9.2	8.0	7.5	0.5	0.5	0.5
11	26.4	23.2	20.1	20.3	20.3	19.4	13.6	14.9	14.0
13	10.5	14.8	9.7	3.9	7.2	4.2	0.5	0.5	0.5
15	19.5	19.6	18.9	15.6	20.3	15.9	13.6	14.9	14.0
17	8.1	0.8	4.2	5.6	0.5	3.4	4.8	1.0	3.9

[a] Quadrupolar splittings are reported in kHz for the β = 0° sample orientation of Y^{5}GWALP23, Y^{19}GWALP23, and $Y^{5,19}$GALP23. Each value is an average of the magnitude observed when β = 0°, and twice the magnitude observed when β = 90°.

[b] Y^{5}GWALP23 values from [22].

Table 3

Semi-static GALA analysis of tyrosine-containing GWALP23-like peptides[a]

	DLPC				DMPC				DOPC			
Peptide	**τ_0**	**ρ_0**	**S_{zz}**	**RMSD (kHz)**	**τ_0**	**ρ_0**	**S_{zz}**	**RMSD (kHz)**	**τ_0**	**ρ_0**	**S_{zz}**	**RMSD (kHz)**
b Y^5	19°	295°	0.78	0.7	10°	300°	0.81	0.39	5°	310°	0.81	0.88
Y^{19}	19°	310°	0.67	1.0	9°	323°	0.87	0.87	5°	336°	0.83	0.77
$Y^{5,19}$	19°	305°	0.58	1.6	9°	311°	0.80	0.37	5°	325°	0.83	0.50

[a] Calculations based on six ^{2}H-Ala methyl quadrupolar splittings.

[b] Values for Y^5GWALP23 from reference [22].

J Phys Chem B. Author manuscript; available in PMC 2014 November 07.

Table 4

Dipolar couplings and ^{15}N chemical shift values for backbone $^{15}N/^{1}H$ groups in $Y^{19}GWALP23$[a]

	$Y^{19}GWALP23$	
Residue	**^{15}N, ppm**	**$^{15}N/^{1}H$, kHz**
13	98.2	2.9
14	91.4	2.3
15	89.0	2.7
16	90.9	3.1
17	98.3	2.6

[a] Samples were measured in magnetically-oriented DMPC-ether/DHPC-ether bicelles where the sample orientation is $\beta = 90°$.

Table 5

Calculated orientations and dynamics of peptides in DMPC[a]

Peptide	Model	τ_0	σ_τ	ρ_0	σ_ρ	S_{zz}	RMSD (kHz)	n[b]
GWALP23	Gaussian	21°	5°	306°	54°	0.88[c]	1.1	16
	semi-static	11°	n.a.[d]	307°	n.a.[d]	0.75	1.2	16
Y^5GWALP23	Gaussian	21°	9°	298°	66°	0.88[c]	1.2	16
	semi-static	12°	n.a.[d]	298°	n.a.[d]	0.73	1.2	16
Y^{19}GWALP23	Gaussian	24°	2°	321°	77°	0.88[c]	1.1	16
	semi-static	11°	n.a.[d]	322°	n.a.[d]	0.72	1.3	16

[a] The Gaussian model for the dynamics uses a fixed principal order parameter S_{ZZ}[35], representing the dynamic extent of (mis)alignment (angle α) between the molecular z-axis and its average orientation, characterized by the time average $S_{ZZ} = \langle 3\cos^2\alpha - 1\rangle/2$[45] Within this context, further motions can be characterized by the widths σ_τ and σ_ρ of Gaussian distributions about the average values of tilt magnitude τ_0 and tilt direction ρ_0[35] . An alternative semi-static analysis, using three parameters instead of four, determines the best fit (lowest RMSD, in kHz) as a function of τ_0, ρ_0 and a variable S_{ZZ}.

[b] Number of data points (from Tables 2, 4), identified as six ^{2}H-Ala methyl quadrupolar couplings, either alone or with five ^{15}N/^{1}H dipolar couplings and five ^{15}N chemical shifts.

[c] Fixed value.

[d] Not applicable.